




 Cite this: *Phys. Chem. Chem. Phys.*, 2024, 26, 7407

# Reactivity of cationic silver clusters with O<sub>2</sub>: a probe of interplay between clusters' geometric and electronic structures†

 Jin Hu, Jun Ma, Zhengqian Jin, Wen Liu, Lulu Huang, Xuefeng Wang \* and Xiaopeng Xing \*

We explored the size-dependent reactivity of Ag<sub>n</sub><sup>+</sup> (*n* = 2–22) with O<sub>2</sub> under mild conditions and found that only a few sizes of Ag<sub>n</sub><sup>+</sup>, with even values of *n* = 4, 6, 12, 16, 18, and 22, are reactive. Possible structures of Ag<sub>n</sub><sup>+</sup> (*n* = 2–22) were determined using a genetic algorithm with incomplete local optimizations at the DFT level, and the calculated bonding strengths of O<sub>2</sub> on these structures are consistent with experimental observations. Analyses revealed a close relationship between the reactivity of Ag<sub>n</sub><sup>+</sup> with O<sub>2</sub> and its HOMO–LUMO gap: cationic silver clusters with a small HOMO–LUMO gap are reactive, which can be rationalized by the covalent character of chemical bonds between Ag<sub>n</sub><sup>+</sup> and O<sub>2</sub> involving their frontier orbitals. The peculiar size-dependent HOMO–LUMO gaps and reactivity with O<sub>2</sub> correlate with the subtle interplay between the electronic configurations and geometric structures of these silver cluster cations.

 Received 19th October 2023,  
 Accepted 26th January 2024

DOI: 10.1039/d3cp05082c

rsc.li/pccp

## 1. Introduction

The geometric and electronic structures of small clusters are fundamental to understanding their properties and exploring their potential applications.<sup>1–4</sup> For a bulk system, the geometric and electronic structures are independent, while the electronic properties of nanoparticles or sub-nano clusters are generally correlated with their geometric structures. Like small molecules, the geometric and electronic structures of sub-nano clusters interplay with each other, which can be rationalized using the Jahn–Teller effect.<sup>5–9</sup> Metal clusters with good ductility and relatively simple electron configurations are ideal examples to explore this interplay, and the free electron shell model applied in these species needs to take their geometric characteristics into account.<sup>10–12</sup>

Silver clusters serve as valuable model systems for investigating the active sites of silver-based catalysts in various

oxidation processes with significant industrial relevance, for example, the partial oxidation of ethylene to ethylene oxide,<sup>13,14</sup> partial oxidation of methanol or ethanol to their aldehydes,<sup>15</sup> and selective oxidation removal of CO from H<sub>2</sub> used in fuel cells.<sup>16,17</sup> In addition, the relatively simple electronic configuration and bonding character of the silver element make silver clusters ideal models for understanding many fundamental concepts in the cluster field. By analyzing the mass spectra of Ag<sub>n</sub><sup>+</sup> and Ag<sub>n</sub> formed in the gas phase, previous investigations showed that the enhanced abundances of certain sizes can be rationalized using the free electron model initially observed in the alkali metal clusters.<sup>18,19</sup> The electronic properties of Ag<sub>n</sub><sup>–</sup> were characterized using photoelectron spectroscopy, and size-dependent electron detachment energies provide evidence for the applicability of the electron shell model in anionic silver systems.<sup>20–22</sup> The geometric structures of some Ag<sub>n</sub><sup>–</sup> and Ag<sub>n</sub><sup>+</sup> species were explored by combining the fingerprint information from various experiments using photoelectron spectroscopy, ion mobility, and trapped ion electron diffraction techniques and theoretical calculations.<sup>21–27</sup>

Reactions between Ag<sub>n</sub><sup>–</sup> and O<sub>2</sub> used as supplemental probes for the electronic properties of anionic silver clusters according to a scenario in which one electron transfers from the anionic silver moiety to the adsorbed O<sub>2</sub> in formed complexes.<sup>28–33</sup> There are drastic changes in the reactivity for sizes of Ag<sub>n</sub><sup>–</sup> containing 8 and 20 free electrons, which implies the formation of electron shells like those in an atom.<sup>30,31</sup> The interplay between the geometric and electronic structures was

School of Chemical Science and Engineering, Shanghai Key Lab of Chemical Assessment and Sustainability, Tongji University, 1239 Siping Road, Shanghai, 200092, China. E-mail: xfwang@tongji.edu.cn, xingxp@tongji.edu.cn

† Electronic supplementary information (ESI) available: The mass spectra of Ag<sub>n</sub><sup>+</sup> (*n* = 1–3) with the presence of O<sub>2</sub> (Fig. S1; PDF); the calculated low-lying structures of Ag<sub>n</sub><sup>+</sup> (*n* = 2–22) (Fig. S2–S10; PDF); the reaction paths of the dominant structures of Ag<sub>n</sub><sup>+</sup> (*n* = 4, 6, 8, 10, 12) with O<sub>2</sub>, the lowest-lying structures of Ag<sub>n</sub>O<sub>2</sub><sup>+</sup> (*n* = 3–12) with O<sub>2</sub> inserted into or dissociated on the silver moiety, the relative energies of multiple products of Ag<sub>10</sub><sup>+</sup> with O<sub>2</sub>, and the bonding scheme of Ag<sub>4</sub>O<sub>2</sub><sup>+</sup> and Ag<sub>6</sub>O<sub>2</sub><sup>+</sup> (Fig. S11–S14; PDF); the schematic experimental setup (Fig. S15; PDF). See DOI: <https://doi.org/10.1039/d3cp05082c>



discussed in sizes containing 14 and 30 free electrons.<sup>30,33</sup> A recent study combining reaction experiments and theoretical calculations showed the remarkable stability of  $\text{Ag}_{17}^-$  due to its closed electronic as well as geometric shells,<sup>32</sup> and a single congener doping atom can result in the rearrangement of the geometry of  $\text{Ag}_{17}^-$  and significantly change its electronic properties and reactivity.<sup>34</sup>

In contrast to the good understanding of the electronic properties of anionic silver clusters and therefore the correlation with the reactivity with  $\text{O}_2$ , there are no efficient techniques to directly characterize the electronic properties of cationic silver clusters. Reactions between  $\text{Ag}_n^+$  and  $\text{O}_2$  species were previously explored in the extension region of the cluster source at low temperatures.<sup>35–39</sup> The results showed a general even–odd oscillation of the reactivity in the size range up to one nanometre. It was proposed that  $\text{Ag}_n^+$  containing 2, 8, and 20 free electrons form closed electron shells, which endows them enhanced stability, and a slight increase of the temperature ( $\sim 105$  K) leads to the dissociation of  $\text{O}_2$  on  $\text{Ag}_n^+$  to form the oxide state of silver.<sup>35,38,39</sup> A recent experiment using an ion trap running at room temperature showed that the even-odd oscillation in the reactivity of  $\text{Ag}_n^+$  ends at  $n = 10$ , and all larger sizes are highly reactive.<sup>40</sup> In these previous experiments, cluster etching paths and reactive odd sizes of  $\text{Ag}_n^+$  are hints that extra energies could be ubiquitous in reaction systems, facilitating the crossing of barriers associated with bond breakages or spin accommodation requirements. The reactivity of clusters under relatively violent conditions could partially mask the effects of their intrinsic geometric or electronic characteristics.

Herein, we explored the reactions of  $\text{Ag}_n^+$  ( $n = 2–22$ ) with  $\text{O}_2$  under mild conditions, in which clusters and reactant  $\text{O}_2$  were pre-cooled by a helium buffer gas before entering the reaction cell, it was ensured that reaction systems were canonical ensembles at a defined low temperature.<sup>31,41</sup> Under conditions described in the Experimental section, a peculiar discontinuous even–odd oscillation was observed for the of reactivity. In addition to the inertness of odd sizes which was attributed to barriers from the spin accommodation requirement,<sup>30</sup> a few even sizes, including  $\text{Ag}_4^+$  and  $\text{Ag}_{10}^+$  which were expected to have alkali-like electron configurations and high reactivity,<sup>36,39</sup> were shown to be inert. Combining these carefully designed experiments and large theoretical calculations, we found that the peculiar discontinuous odd–even oscillation of the reactivity of clusters reflects the size-dependent feasibility of the transition from physisorption to chemisorption of the combined  $\text{O}_2$ . This feasibility closely correlates with the varying HOMO–LUMO gaps of  $\text{Ag}_n^+$ , which reflect a subtle interplay between their electronic and geometric structures.

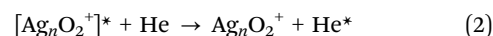
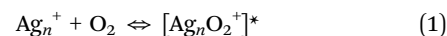
## 2. Experimental and computational methods

The cluster reaction experiments were carried out using an instrument composed of a magnetron sputtering cluster source, a continuous micro tube reactor and a time-of-flight

(TOF) mass spectrometer. The device diagram is shown in Fig. S15 (ESI<sup>†</sup>), and the details of this instrument were described elsewhere.<sup>31,42</sup> Briefly, the cluster source has a liquid-nitrogen-cooled aggregation chamber enclosing a magnetron sputter discharge head. A small tube reactor was installed at the exit of the source chamber, which is isolated from the source by a ceramic spacer. The temperature of this tube reactor was adjusted using a controlled heater and was stabilized at 150 K in this work.

The clusters formed inside the source chamber were carried by the helium buffer gas and argon discharging gas (110 sccm and 14 sccm, respectively) and flowed into the tube reactor. Only those species near the central axis can enter the reaction region, and most clusters were filtered by multi-layer meshes. The intentional decrease in the concentration of metal species in the reaction region is to stop the cluster growth processes. Another function of the multi-layer meshes is to thermalize the carrier gas to the set temperature of the reactor. The reactant  $\text{O}_2$  was introduced through two copper tubes extending close to the axial center of the reactor, which were also thermalized to the temperature of the reactor inside the mantle layer. The flow rates were about 0.02–0.2 sccm. The total pressure inside the aggregation chamber of the cluster source and tube reactor was about 0.5 torr, and the partial pressure of the reactant in the reactor was around  $10^{-4}$  torr. The reaction time was estimated to be several milliseconds. The generated species, including parent clusters and reaction products, went through a skimmer at the end of the flow reactor. The continuous ion beam from the skimmer was directed to and analyzed using a time-of-flight (TOF) mass spectrometer operating at 800 Hz. The mass spectra of species at a series of  $\text{O}_2$  flow rates were recorded using the TOF mass spectrometer. The intensity of one parent cluster  $\text{Ag}_n^+$  at a certain  $\text{O}_2$  flow rate ( $I$ ) and that without  $\text{O}_2$  ( $I_0$ ) were separately integrated.

The adsorption process of clusters and  $\text{O}_2$  molecules follows the Lindemann reaction mechanism. Taking  $\text{Ag}_n^+$  and  $\text{O}_2$  as an example:



and the reaction rate can be written in the following form:

$$\frac{dI}{dt} = k_{\text{III}}[\text{O}_2][\text{He}]I \quad (3)$$

Integrate both sides to get:

$$-\ln \frac{I}{I_0} = k_{\text{III}}[\text{O}_2][\text{He}]t \quad (4)$$

The rate constant  $k_{\text{III}}$  is proportional to  $-\ln(I/I_0)/n$  since true concentrations of  $\text{O}_2$  and He (shown as  $[\text{O}_2]$  and  $[\text{He}]$ ) and the reaction time  $t$  are constant. Besides,  $[\text{O}_2]$  and  $[\text{He}]$  are much larger than the partial pressure of metal clusters, so the reaction can be regarded as a quasi-first-order reaction. We plotted the obtained  $-\ln(I/I_0)$  vs. the flow of  $\text{O}_2$ , and the slope of the resulting straight line is proportional to  $k_{\text{III}}$ .



The structure search of silver clusters was conducted using our newly encoded genetic algorithm program with an incomplete local optimization strategy,<sup>33</sup> in which all optimization processes and energy calculations were carried out using the Gaussian09 program.<sup>43</sup> Briefly, we used a module to generate random structures including, a space-free motif, a close packing motif, a simple cubic packing motif, a cage motif, a solid sphere motif, a ring motif and other user-defined motifs. These structures were screened according to their calculated energies and evolved toward low-lying ones through multiple rounds of crossovers, mutations, and competitions. The main feature of this program is that all local optimizations in the structure evolution are terminated in a relatively flat area rather than exact local minimum points on the potential energy surface (PES), and only the structures of the last generation were completely optimized to obtain the global minimum. The efficiency and reliability of methods have been previously shown in searching the structure of Ag<sub>30</sub> and other representative clusters.<sup>33</sup> The initial structural candidates of Ag<sub>n</sub>O<sub>2</sub><sup>+</sup> reaction products were generated by randomly putting O<sub>2</sub> around all possible adsorption sites of obtained lowest-lying structures of Ag<sub>n</sub><sup>+</sup>, and various adsorption patterns including O-atop and O–O doubly connected geometries in their doublet or quartet state were considered. The complete and incomplete optimizations in this study were at the PBE level with the def2-SVP basis set for Ag and def2-TZVP basis sets for O.<sup>44–46</sup> After each

complete optimization process, the harmonic vibrational frequencies were calculated to confirm that a real minimum point was obtained, and at the same time, the zero-point vibrational energy (ZPVE) was derived. Calculations on the relative energies of various isomers and O<sub>2</sub> adsorption energies were based on the electronic energies of related species modified by their ZPVE corrections. The NPA charges and spin populations on O–O in the obtained structures of Ag<sub>n</sub>O<sub>2</sub><sup>+</sup> were calculated.

### 3. Results and discussion

#### 3.1 Size-dependent reactivity of Ag<sub>n</sub><sup>+</sup> (*n* = 2–22) with O<sub>2</sub>

Fig. 1a shows Ag<sub>n</sub><sup>+</sup> (*n* = 4–23) species formed in the cluster source and their reaction products with 0.025 sccm and 0.075 sccm O<sub>2</sub>. The vertical dashed lines indicate Ag<sub>n</sub><sup>+</sup>, and circle symbols indicate dominant products, such as Ag<sub>n</sub>O<sub>2</sub><sup>+</sup>. For Ag<sub>n</sub><sup>+</sup> (*n* < 4), the mass spectra contained cluster complexes with argon from the sputter source and nitrogen or CO molecules possibly from the background. However, the spectra clearly show that there were no oxygen-adsorbed products for Ag<sub>n</sub><sup>+</sup> (*n* = 1–3) (shown in Fig. S1, ESI<sup>†</sup>). The relative kinetic rates of Ag<sub>n</sub><sup>+</sup> were obtained as described in the Experimental section, and are summarized in Fig. 1b. The reactivity showed an apparent even-odd oscillation, in which all active sizes contain an even number of atoms, in other words, an odd number of valence

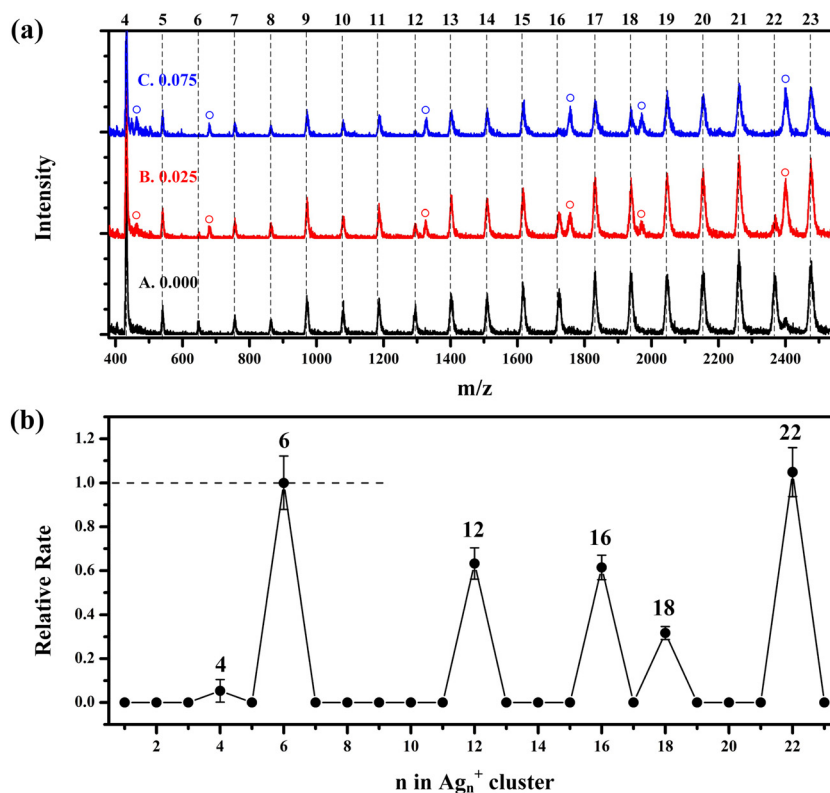


Fig. 1 (a) Mass spectra of parent and product ions for reactions between Ag<sub>n</sub><sup>+</sup> (*n* = 4–23) and O<sub>2</sub> with O<sub>2</sub> flows of 0.000 sccm (curve A), 0.025 sccm (curve B) and 0.075 sccm (curve C) at 150 K. Dot lines in the mass spectra indicate the positions of Ag<sub>n</sub><sup>+</sup>, and circle symbols indicate dominant products, such as Ag<sub>n</sub>O<sub>2</sub><sup>+</sup>. (b) Relative reaction rates normalized to that of Ag<sub>6</sub><sup>+</sup>. Detection limit of relative rates was estimated to be 10<sup>-2</sup>.



electrons. All reactive sizes adsorbed only one  $O_2$ . Notably, not all even sizes in this range showed detectable activity.  $Ag_n^+$  species with  $n = 8, 10, 14,$  and  $20$  are inert, and the reactivity of  $n = 4$  is very low, which is different from previous experimental observations.<sup>36,39,40</sup>

### 3.2 Theoretical structures and electronic properties of $Ag_n^+$ ( $n = 2-22$ )

To understand the peculiar discontinuous odd-even oscillation of the reactivity, we theoretically explored structural candidates of  $Ag_n^+$  ( $n = 2-22$ ) using a newly developed genetic algorithm program<sup>33</sup> and determined the most likely ones according to their relative energies and comparisons with the results from previous experiments. The low-lying isomers for each size of  $Ag_n^+$  ( $n = 2-22$ ) are displayed in Fig. S2–S10 (ESI<sup>†</sup>), and the most likely ones present in experiments are presented in Fig. 2a. The structures of  $Ag_n^+$  ( $n = 2-13$ ) were recently determined based on a combination of the far-infrared multiple photon dissociation spectra of the complexes of clusters and theoretical calculations.<sup>41</sup> The lowest-lying structures of  $Ag_n^+$  ( $n = 2-5, 8, 10-13$ ) from our calculations (Fig. S2–S6, ESI<sup>†</sup>) are consistent with this report. The results of  $Ag_6^+, Ag_7^+$  and  $Ag_9^+$  in our calculations (Fig. S2–S4, ESI<sup>†</sup>) include

one or two structures with even lower energies at the present theoretical level, while energy differences are almost negligible. The results of  $Ag_n^+$  ( $n = 12-15$ ) (Fig. S5–S7, ESI<sup>†</sup>) are in complete agreement with those in previous theoretical studies.<sup>47-50</sup> The minimum structure of optimized  $Ag_{19}^+$  (Fig. S9, ESI<sup>†</sup>) is consistent with the one previously determined using trapped ion electron diffraction experiments and theoretical calculations.<sup>27</sup> For  $n = 16, 17, 18$  and  $20$  (Fig. S7–S9, ESI<sup>†</sup>), we found one or two new structures with lower energies than those from a previous theoretical report.<sup>49</sup> For  $n = 21$  and  $22$  (Fig. S10, ESI<sup>†</sup>), our calculation found more than seven isomers which are more stable than the lowest-lying ones reported by previous theoretical studies.<sup>49,50</sup> In Fig. 2a, we list the structures of  $Ag_n^+$  ( $n = 3-13$ ) previously confirmed by the combined experiment and theoretical calculation<sup>41</sup> and the lowest-lying ones of  $Ag_n^+$  ( $n = 14-22$ ) from our calculations. We saw that the shapes of clusters vary with increasing size: the structures undergo a 2D ( $n = 4$ ) to 3D ( $n = 5$ ) transition and become near-spherical at  $n = 8$  and  $9$ ; the structures of  $n = 10-14$  have elongated prolate shapes and those of  $n = 15-17$  display an oblate sheet formed by two layers of staggered atoms; for sizes with  $n = 17-19$ , geometries change into an irregular

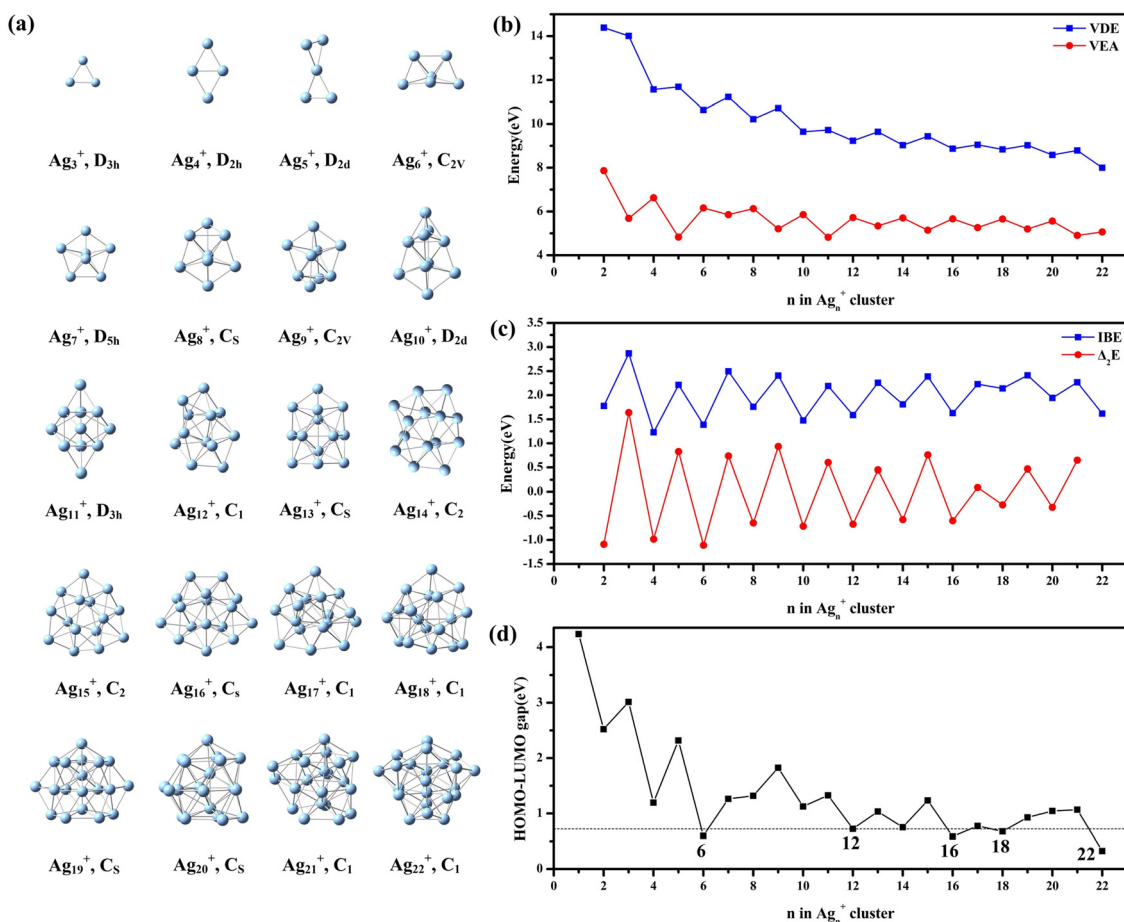


Fig. 2 (a) Structures of  $Ag_n^+$  ( $n = 3-22$ ) predicted by calculations at the PBE/def2-SVP level of theory, and their theoretical properties including (b) vertical detachment energies (VDE) and vertical electron affinities (VEA), (c) incremental binding energies (IBE) and the second-order difference in binding energies ( $\Delta_2E$ ), and (d) HOMO–LUMO (H–L) gaps. Structures of  $Ag_n^+$  ( $n = 3-13$ ) were determined by comparisons between low-lying structures and the available experimental information. Structures of  $Ag_n^+$  ( $n = 14-22$ ) were proposed to be the lowest-lying ones in calculations.



oblate shape with an embedded silver atom; for those with  $n = 20$ – $22$ , all atoms are tightly packed into a quasi-spherical shape and the number of silver atoms trapped inside increases to two or three.

We calculated the electronic and energetic features of the most likely structures shown in Fig. 2a, including vertical electron detachment energies (VDE), vertical electron affinities (VEA), the incremental binding energies (IBE), and second-order differences in binding energy ( $\Delta_2E$ ), which were defined as follows:

$$\text{VDE}(\text{Ag}_n^+) = E[\text{Ag}_n^{2+}] - E[\text{Ag}_n^+] \quad (5)$$

$$\text{VEA}(\text{Ag}_n^+) = E[\text{Ag}_n^+] - E[\text{Ag}_n^0] \quad (6)$$

$$\text{IBE}(\text{Ag}_n^+) = E[\text{Ag}^0] + E[\text{Ag}_{n-1}^+] - E[\text{Ag}_n^+] \quad (7)$$

$$\Delta_2E(\text{Ag}_n^+) = E[\text{Ag}_{n+1}^+] + E[\text{Ag}_{n-1}^+] - 2E[\text{Ag}_n^+] \quad (8)$$

As seen in Fig. 2b, there is a general odd–even oscillation in VDE and VEA. For VDE, a high value of odd-sized  $\text{Ag}_n^+$  species is due to their lower-energy singlet state formed by an even number of electrons, compared to its even-size neighbors with one unpaired electron. Note that with an increase of  $n$ , the variation of VDE gradually becomes smooth, but significantly decreases at  $\text{Ag}_{22}^+$  (0.58 eV lower than  $\text{Ag}_{20}^+$  and 0.78 eV lower than  $\text{Ag}_{21}^+$ ). VEA is reminiscent of a mirror image of VDE, with a large VDE corresponding to a small VEA. Comparing Fig. 1 and Fig. 2b, we see no evident correlation between the reactivity of  $\text{Ag}_n^+$  species with oxygen and their VDEs or VEAs, which is different from the case observed for silver cluster anions.<sup>30–32</sup>

IBE and  $\Delta_2E$  are depicted in Fig. 2c, both of which show oscillatory trends and do not have a correlation with the reactivity in Fig. 1. HOMO–LUMO gaps in Fig. 2d exhibit a large drop from  $\text{Ag}_3^+$  to  $\text{Ag}_{22}^+$ . Additionally, it was found that there is a threshold of about 0.73 eV that separates reactive clusters from inert ones observed in Fig. 1. Especially, the significantly lower HOMO–LUMO gap and VDE of  $\text{Ag}_{22}^+$  than those other species correspond to a greater propensity to adsorb one  $\text{O}_2$  in experiments, whereas  $\text{Ag}_{20}^+$ , with an open-shell size, unexpectedly shows a sizable gap, even larger than its neighbor  $\text{Ag}_{19}^+$ , with a closed 18-electron shell.

### 3.3 Theoretical exploration of the bonding of $\text{O}_2$ on $\text{Ag}_n^+$ ( $n = 2$ – $22$ )

We theoretically explored the structures of  $\text{Ag}_n\text{O}_2^+$  ( $n = 3$ – $12$ ,  $20$ , and  $22$ ) and bonding strengths of adsorbed  $\text{O}_2$ . The structure searching started from the structures of  $\text{Ag}_n^+$  ( $n = 3$ – $22$ ) shown in Fig. 2, and one  $\text{O}_2$  unit was put on each adsorption site in an end-on or side-on manner. Then, all convergent structures were sequenced according to their energies. For all even- and odd-sized clusters, calculations located structures with an end-on  $\text{O}_2$ . There are also some structures for even sizes with a side-on  $\text{O}_2$ , while no such ones for odd sizes. The lowest-lying structures of  $\text{Ag}_n\text{O}_2^+$  ( $n = 3$ – $12$ ,  $20$ , and  $22$ ) with an end-on  $\text{O}_2$  and those of the  $\text{Ag}_n\text{O}_2^+$  ( $n = 4$ ,  $6$ ,  $8$ ,  $10$ ,  $12$ ,  $20$ , and  $22$ ) with a side-on  $\text{O}_2$  are shown in Fig. 3a and b, respectively. For nearly all structures with either an end-on or a side-on  $\text{O}_2$ , silver moieties

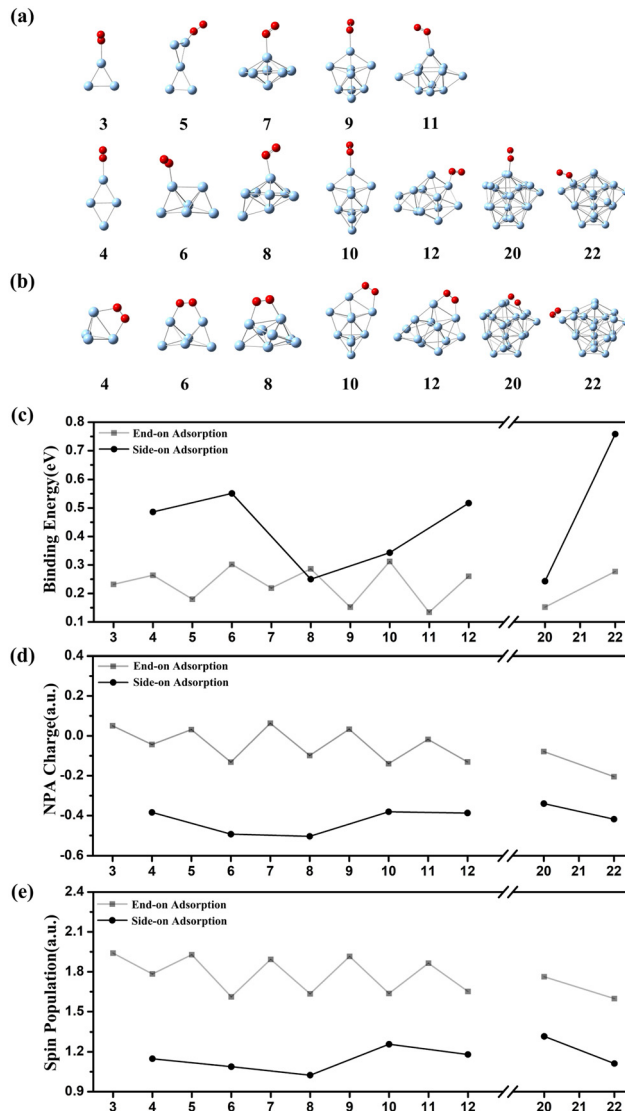


Fig. 3 (a) Structures of  $\text{Ag}_n\text{O}_2^+$  ( $n = 3$ – $12$ ,  $20$ , and  $22$ ) containing an end-on  $\text{O}_2$  and (b)  $\text{Ag}_n\text{O}_2^+$  ( $n = 4$ ,  $6$ ,  $8$ ,  $10$ ,  $12$ ,  $20$ , and  $22$ ) containing a side-on  $\text{O}_2$  formed by  $\text{Ag}_n^+$  structures shown in Fig. 2; the calculated properties of above structures including (c) the binding energy of  $\text{O}_2$ , (d) NPA charges on  $\text{O}_2$ , and (e) spin populations on  $\text{O}_2$ . All structures and their properties are from calculations at the PBE level with the def2-SVP basis set for Ag and def2-TZVP basis set for O.

remain the original geometries of  $\text{Ag}_n^+$ . The only exception is the lowest-lying  $\text{Ag}_4\text{O}_2^+$  in Fig. 3b, in which the frame of  $\text{Ag}_4^+$  changes from a rhomboid to a pyramid after combining with a side-on  $\text{O}_2$ . The binding energy of  $\text{O}_2$  in each structure and charge and spin populations localized on the  $\text{O}_2$  unit are shown in Fig. 3c–e. In Fig. 3c, the bonding energies of side-on  $\text{O}_2$  on  $\text{Ag}_n^+$  ( $n = 4$ ,  $6$ ,  $12$ , and  $22$ ) are higher than 0.4 eV and those of side-on  $\text{O}_2$  on  $\text{Ag}_n^+$  ( $n = 8$ ,  $10$ , and  $20$ ) are lower than 0.35 eV; the bonding energies of end-on  $\text{O}_2$  on all even or odd sizes are lower than 0.35 eV. These calculated binding energy values are generally consistent with experimental observations in Fig. 1, since the threshold of the binding energy to resist the entropy decrease accompanying the adsorption was estimated to be



around 0.37 eV under similar experimental condition.<sup>51</sup> In Fig. 3d, there are very small amounts of negative charge (<0.2 a.u.) populated on end-on O<sub>2</sub>, while the amounts on side-on O<sub>2</sub> in even sizes are apparently larger. In Fig. 3e, the spin populations on side-on O<sub>2</sub> are 1.6–2.0 a.u., while those on end-on O<sub>2</sub> are 1.0–1.3 a.u. These apparently different charge and spin values imply that end-on and side-on O<sub>2</sub> are in different states. To summarize the findings from bonding energies and charge and spin populations, end-on O<sub>2</sub> units are physisorbed and side-on O<sub>2</sub> units found in even sizes are chemically bonded. The transition paths from the end-on state to the side-on state of O<sub>2</sub> in Ag<sub>n</sub><sup>+</sup> (*n* = 4, 6, 8, 10, and 12) were theoretically explored, and the results are shown in Fig. S11a–e (ESI†). It is interesting to find that the variation of the kinetic barriers of the transitions of these five sizes is consistent with the changes of their HOMO–LUMO gaps, which are summarized in Fig. S11f (ESI†). These trends are also consistent with the observed reactivity variation shown in Fig. 1. Especially, the calculated high binding energy (0.48 eV) of O<sub>2</sub> on Ag<sub>4</sub><sup>+</sup> in Fig. 3c, and the small amounts of reacted Ag<sub>4</sub><sup>+</sup> in Fig. 1 can be rationalized using the kinetic barrier for the transition from the rhomboid to the pyramid of the silver frame or the presence of a tiny amount of the reactive pyramid isomer.

We also explored the structures of Ag<sub>n</sub>O<sub>2</sub><sup>+</sup> without restrictions that the two oxygen atoms connect together and silver clusters are maintained as one unit. The lowest-lying structures of this kind are shown in Fig. S12 (ESI†). The new structures determined for Ag<sub>n</sub>O<sub>2</sub><sup>+</sup> (*n* = 3–7) have higher energies than or energies very close to the ones shown in Fig. 3a. The energies of all even- and odd-sized Ag<sub>n</sub>O<sub>2</sub><sup>+</sup> (*n* = 8–12) in Fig. S12 (ESI†) are apparently lower than those of their structures in Fig. 3a, and the energy decreases from separate Ag<sub>n</sub><sup>+</sup> and O<sub>2</sub> to these structures are much larger than the estimated threshold (~0.37 eV) resisting the entropy decrease. The completely different trends of these reaction energies in Fig. S12 (ESI†), and the reactivity shown in Fig. 1 imply that the dissociation of O<sub>2</sub> is less likely under present mild conditions. Using the reaction of Ag<sub>10</sub><sup>+</sup> with O<sub>2</sub> as an example, we also considered reaction energies for possible etching reaction channels, which include those reported in previous experiments.<sup>35–39</sup> The results shown in Fig. S13 (ESI†) indicate that all etching or dissociation channels are highly endothermic and cannot happen under present mild conditions.

The correlation between the H–L gap of Ag<sub>n</sub><sup>+</sup> clusters and their reactivity to oxygen revealed in this study is in contrast to the reactivity of Ag<sub>n</sub><sup>−</sup> highly correlated with the VDE of clusters. The varying reactivity of anionic silver clusters with O<sub>2</sub> was generally attributed to two reasons:<sup>30–32,42,52</sup> (1) the stable reaction products of odd-sized IB metal cluster anions (singlet) with O<sub>2</sub> (triplet) are in a singlet state, and there are always barriers related to the spin accommodation requirement in these reaction systems; (2) even-size IB metal cluster anions with lower electron detachment potentials are generally reactive, because their electronic properties facilitate the directed transfer of the unpaired electron from the metal moiety to bonded O<sub>2</sub>. In previous studies of the reactions between Ag<sub>n</sub><sup>+</sup> and O<sub>2</sub>,<sup>35–39</sup> observed Ag<sub>n</sub>O<sub>2</sub><sup>+</sup> complexes were considered to be

a combination of Ag<sub>n</sub><sup>2+</sup> and O<sub>2</sub><sup>−</sup> through ionic bonding, where electron transfer similar to that in anionic silver or gold clusters was proposed. Following this assumption, the VDE value of clusters should be qualitatively consistent with their reactivity to O<sub>2</sub>, as well as the amount of charge transfer from the cluster to the O<sub>2</sub> subunit. However, in the present study, there seems to be no apparent correlation between VDE values in Fig. 2b and NPA values in Fig. 3d or HOMO–LUMO gaps in Fig. 2d. The superatomic features in Fig. 4 cannot be associated with VDE values either. Instead, the exclusive dominance of H–L gaps of clusters on the reactivity was revealed, suggesting that the interaction in Ag<sub>n</sub>O<sub>2</sub><sup>+</sup> involves HOMO and LUMO of Ag<sub>n</sub><sup>+</sup>. We show orbital interactions of the silver moiety and O<sub>2</sub> molecule using two representative complexes, Ag<sub>4</sub>O<sub>2</sub><sup>+</sup> and Ag<sub>6</sub>O<sub>2</sub><sup>+</sup>, in Fig. S14(a) and (b) (ESI†), respectively. In these two cases, the interaction between Ag<sub>n</sub><sup>+</sup> and O<sub>2</sub> can be considered as follows: the single electron on the HOMO of Ag<sub>n</sub><sup>+</sup> was excited to its LUMO, and the combination of this LUMO and one π<sub>g</sub> of O<sub>2</sub> formed the bonding orbital in Ag<sub>n</sub>O<sub>2</sub><sup>+</sup>. In a certain sense, this interaction has a covalent character.

### 3.4 Interplay between geometries and HOMO–LUMO gaps of Ag<sub>n</sub><sup>+</sup> (*n* = 2–22)

An unexpected phenomenon in this study is the size-dependence of HOMO–LUMO gaps and therefore the reactivity of even sizes Ag<sub>n</sub><sup>+</sup>, which in many points are in marked contrast to the prediction of the free electron shell model.<sup>10</sup> For example, even-sized Ag<sub>4</sub><sup>+</sup> and Ag<sub>10</sub><sup>+</sup> have one more electron than closed shells composed of 2 and 8 electrons, respectively, and therefore are expected to be like alkali metal atoms with small HOMO–LUMO gaps and high reactivity with O<sub>2</sub>. This expectation is true for anionic Ag<sub>2</sub><sup>−</sup> (*n<sub>e</sub>* = 2 + 1)<sup>29,53</sup> and Ag<sub>8</sub><sup>−</sup> (*n<sub>e</sub>* = 8 + 1),<sup>54</sup> both of which are quite reactive with O<sub>2</sub>. However, experiments and calculations in this study showed that Ag<sub>4</sub><sup>+</sup> and Ag<sub>10</sub><sup>+</sup> have large HOMO–LUMO gaps and have low reactivity or are completely inert. The decrease of HOMO–LUMO gaps and the increase of the reactivity from Ag<sub>4</sub><sup>+</sup> to Ag<sub>6</sub><sup>+</sup> and from Ag<sub>10</sub><sup>+</sup> to Ag<sub>12</sub><sup>+</sup> are also unexpected. Ag<sub>20</sub><sup>+</sup> and Ag<sub>22</sub><sup>+</sup> are expected to have electron configurations like those of alkali metals, because they have one more electron than closed shells composed of 18 and 20 free electrons, respectively. However, Ag<sub>20</sub><sup>+</sup> is found to have a quite large HOMO–LUMO gap and no reactivity with O<sub>2</sub>. In Fig. 4, we plot energy levels of three pairs of even-sized species around unexpected turning points (Ag<sub>4</sub><sup>+</sup> → Ag<sub>6</sub><sup>+</sup>; Ag<sub>10</sub><sup>+</sup> → Ag<sub>12</sub><sup>+</sup>; Ag<sub>20</sub><sup>+</sup> → Ag<sub>22</sub><sup>+</sup>). For Ag<sub>4</sub><sup>+</sup>, the lowest-lying rhomboid structure (in Fig. 2) and pyramid structure (an isomer 0.32 eV higher; shown in Fig. S2, ESI†) were considered, since chemisorbed O<sub>2</sub> on the rhomboid structure of Ag<sub>4</sub><sup>+</sup> changed it to the pyramid one (shown in Fig. 3 and Fig. S11, ESI†). The energy levels and orbital shapes of pyramid Ag<sub>4</sub><sup>+</sup> in Fig. 4a show that its three 1p orbitals are very close, and the electron configuration 1s<sup>2</sup>1p<sup>1</sup> leads to a very small HOMO–LUMO gap. The rhomboid Ag<sub>4</sub><sup>+</sup> (in Fig. 4a) has only two 1p orbitals because of its planar potential field,<sup>11</sup> and the energies of these two orbitals are well separated because of the apparent difference between the two diagonals of the rhomboid. The 1p orbital along the longer diagonal is lower in



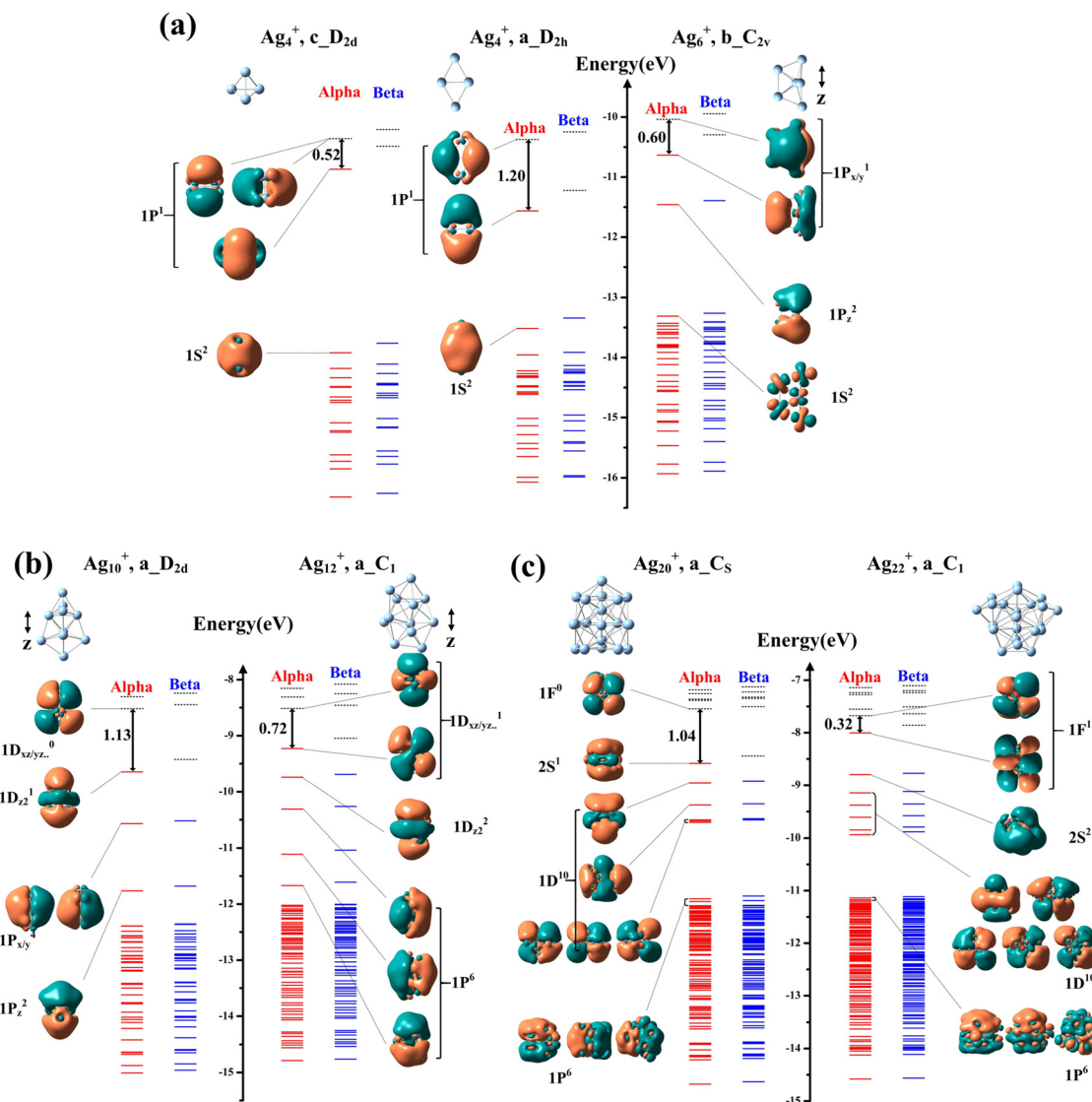


Fig. 4 Orbital levels in (a)  $\text{Ag}_4^+$  (pyramid and rhomboid symmetries) and  $\text{Ag}_6^+$ , (b)  $\text{Ag}_{10}^+$  and  $\text{Ag}_{12}^+$ , and (c)  $\text{Ag}_{20}^+$  and  $\text{Ag}_{22}^+$ . In each panel, red and the blue solid lines indicate occupied alpha and beta orbitals, respectively. Black dashed lines indicate unoccupied orbitals. The shapes of some orbitals around HOMOs and LUMOs are shown, and the isosurface value is  $\pm 0.005$  a.u. The naming of the orbitals was based on the free electron shell model. HOMO–LUMO gaps of alpha levels are indicated.

energy and the other along the shorter diagonal is higher. The geometries of  $\text{Ag}_6^+$  (Fig. 4a),  $\text{Ag}_{10}^+$  and  $\text{Ag}_{12}^+$  (Fig. 4b) can roughly be viewed as a 3D structure extending longer in one direction (labeled as the  $z$  direction using arrows beside structures in Fig. 4) than other two orthogonal ones ( $x/y$ ). Based on quantum mechanical figures, the orbital extending to the longer direction tends to be lower in energy than others of the same type. In  $\text{Ag}_6^+$  (Fig. 4a), the electron configuration is  $1s^2 1p_z^2 1p_{x/y}^1$ , and the small energy difference between  $1p_x$  and  $1p_y$  leads to a small HOMO–LUMO gap. In  $\text{Ag}_{10}^+$  (Fig. 4b), the electron configuration is  $1s^2 1p_z^2 1p_{x/y}^4 1d_{z^2}^1 1d_{xy/yz/\dots}^1$ , and the large separation between  $1d_{z^2}$  and other  $1d_{xy/yz/\dots}$  orbitals leads to a large HOMO–LUMO gap. In  $\text{Ag}_{12}^+$  (Fig. 4b), the electron configuration is  $1s^2 1p_z^2 1p_x^2 1p_y^2 1d_{z^2}^1 1d_{xy/yz/\dots}^1$  and the relatively small energy differences among  $1d_{xy/yz/\dots}$  orbitals lead to a small HOMO–LUMO

gap. For  $\text{Ag}_{20}^+$  and  $\text{Ag}_{22}^+$  (Fig. 4c), the differences among their  $x/y/z$  dimensions are insignificant, and the splitting of orbitals of the same type is relatively small. The electron configurations of  $\text{Ag}_{20}^+$  and  $\text{Ag}_{22}^+$  are  $1s^2 1p^6 1d^{10} 2s^1$  and  $1s^2 1p^6 1d^{10} 2s^2 1f^1$ , respectively, and their HOMO–LUMO gaps correspond to the large gap between  $2s$  and  $1f$  shells and small gap between two  $1f$  orbitals, respectively.

## 4. Conclusions

We presented a study on reactions of  $\text{Ag}_n^+$  ( $n = 2\text{--}22$ ) with  $\text{O}_2$  by combining experimental measurements and theoretical calculations. Under mild conditions, the reactivity of  $\text{Ag}_n^+$  showed a peculiar size dependence, in which only  $\text{Ag}_n^+$  species



( $n = 4, 6, 12, 16, 18,$  and  $22$ ) are reactive. The most likely structures of  $\text{Ag}_n^+$  ( $n = 2-22$ ) are determined using an improved genetic algorithm and a density functional theory method. The bonding strengths of  $\text{O}_2$  on the determined structures of  $\text{Ag}_n^+$  ( $n = 2-22$ ) are consistent with experimental observations. Analyses of the electronic character of  $\text{Ag}_n^+$  ( $n = 2-22$ ) species indicated that their reactivity with  $\text{O}_2$  is closely related to their HOMO–LUMO gaps. Theoretical results showed that decreased HOMO–LUMO gaps facilitated the formation of covalent interactions with  $\text{O}_2$  under thermodynamic and kinetic considerations. The variation of HOMO–LUMO gaps and therefore the reactivity with  $\text{O}_2$  was further attributed to a subtle interplay between electronic configurations and geometric structures of  $\text{Ag}_n^+$ .

## Conflicts of interest

There are no conflicts to declare.

## Acknowledgements

This work was supported by the National Natural Science Foundation of China (Grant No. 22273065, 21673158) and Science & Technology Commission of Shanghai Municipality (14DZ2261100). Theoretical calculations were carried out on the computing resource in National Supercomputing Center in Shenzhen.

## Notes and references

- S. M. Lang and T. M. Bernhardt, *Phys. Chem. Chem. Phys.*, 2012, **14**, 9255–9269.
- L.-M. Wang and L.-S. Wang, *Nanoscale*, 2012, **4**, 4038–4053.
- Z. X. Luo, A. W. Castleman and S. N. Khanna, *Chem. Rev.*, 2016, **116**, 14456–14492.
- P. Ferrari, J. Vanbuel, E. Janssens and P. Lievens, *Acc. Chem. Res.*, 2018, **51**, 3174–3182.
- J. L. Martins, J. Buttet and R. Car, *Phys. Rev. B: Condens. Matter Mater. Phys.*, 1985, **31**, 1804–1816.
- M. Castro, C. Jamorski and D. R. Salahub, *Chem. Phys. Lett.*, 1997, **271**, 133–142.
- W. Satula, J. Dobaczewski and W. Nazarewicz, *Phys. Rev. Lett.*, 1998, **81**, 3599–3602.
- M. A. Tofanelli, K. Salorinne, T. W. Ni, S. Malola, B. Newell, B. Phillips, H. Hakkinen and C. J. Ackerson, *Chem. Sci.*, 2016, **7**, 1882–1890.
- Q. Y. Du, X. Wu, P. J. Wang, D. Wu, L. W. Sai, R. B. King, S. J. Park and J. J. Zhao, *J. Phys. Chem. C*, 2020, **124**, 7449–7457.
- W. A. Deheer, *Rev. Mod. Phys.*, 1993, **65**, 611–676.
- H. Hakkinen, *Adv. Phys.: X*, 2016, **1**, 467–491.
- T. Tsukamoto, T. Kambe, T. Imaoka and K. Yamamoto, *Nat. Rev. Chem.*, 2021, **5**, 338–347.
- R. M. Lambert, F. J. Williams, R. L. Cropley and A. Palermo, *J. Mol. Catal. A: Chem.*, 2005, **228**, 27–33.
- Y. Lei, F. Mehmood, S. Lee, J. Greeley, B. Lee, S. Seifert, R. E. Winans, J. W. Elam, R. J. Meyer, P. C. Redfern, D. Teschner, R. Schlogl, M. J. Pellin, L. A. Curtiss and S. Vajda, *Science*, 2010, **328**, 224–228.
- H. I. Mahdi, N. N. Ramlee, D. H. D. Santos, D. A. Giannakoudakis, L. H. de Oliveira, R. Selvasembian, N. I. W. Azelee, A. Bazargan and L. Meili, *Mol. Catal.*, 2023, **537**, 112944.
- V. V. Dutov, G. V. Mamontov, V. I. Zaikovskii, L. F. Liotta and O. V. Vodyankina, *Appl. Catal., B*, 2018, **221**, 598–609.
- Z. P. Qu, M. Cheng, C. Shi and X. Bao, *J. Mol. Catal. A: Chem.*, 2005, **239**, 22–31.
- I. Katakuse, T. Ichihara, Y. Fujita, T. Matsuo, T. Sakurai and H. Matsuda, *Int. J. Mass Spectrom. Ion Processes*, 1985, **67**, 229–236.
- G. Alameddin, J. Hunter, D. Cameron and M. M. Kappes, *Chem. Phys. Lett.*, 1992, **192**, 122–128.
- K. J. Taylor, C. L. Pettiette-Hall, O. Cheshnovsky and R. E. Smalley, *J. Chem. Phys.*, 1992, **96**, 3319.
- H. Handschuh, C. Y. Cha, P. S. Bechthold, G. Ganteför and W. Eberhardt, *J. Chem. Phys.*, 1995, **102**, 6406–6422.
- K. Majer and B. von Issendorff, *Phys. Chem. Chem. Phys.*, 2012, **14**, 9371–9376.
- P. Weis, T. Bierweiler, S. Gilb and M. M. Kappes, *Chem. Phys. Lett.*, 2002, **355**, 355–364.
- H. Hakkinen, M. Moseler, O. Kostko, N. Morgner, M. A. Hoffmann and B. von Issendorff, *Phys. Rev. Lett.*, 2004, **93**, 093401.
- X. P. Xing, R. M. Danell, I. L. Garzon, K. Michaelian, M. N. Blom, M. M. Burns and J. H. Parks, *Phys. Rev. B: Condens. Matter Mater. Phys.*, 2005, **72**, 081405.
- D. Schooss, M. N. Blom, J. H. Parks, B. von Issendorff, H. Haberland and M. M. Kappes, *Nano Lett.*, 2005, **5**, 1972–1977.
- M. N. Blom, D. Schooss, J. Stairs and M. M. Kappes, *J. Chem. Phys.*, 2006, **124**, 244308.
- T. H. Lee and K. M. Ervin, *J. Phys. Chem.*, 1994, **98**, 10023–10031.
- J. Hagen, L. D. Socaciu, J. LeRoux, D. Popolan, T. M. Bernhardt, L. Woste, R. Mitric, H. Noack and V. Bonacic-Koutecky, *J. Am. Chem. Soc.*, 2004, **126**, 3442–3443.
- Z. X. Luo, G. U. Gamboa, J. C. Smith, A. C. Reber, J. U. Reveles, S. N. Khanna and A. W. Castleman, *J. Am. Chem. Soc.*, 2012, **134**, 18973–18978.
- J. Ma, X. Cao, X. Xing, X. Wang and J. H. Parks, *Phys. Chem. Chem. Phys.*, 2016, **18**, 743–748.
- B. Q. Yin, Q. Y. Du, L. J. Geng, H. Y. Zhang, Z. X. Luo, S. Zhou and J. J. Zhao, *CCS Chem.*, 2021, **3**, 219–229.
- W. Liu, L. L. Huang, L. Meng, J. Hu and X. P. Xing, *Phys. Chem. Chem. Phys.*, 2023, **25**, 14303–14310.
- Q. Y. Du, L. L. Huang, J. Q. Fu, Y. J. Cao, X. P. Xing and J. J. Zhao, *J. Chem. Phys.*, 2023, **158**, 014306.
- M. Schmidt, P. Cahuzac, C. Brechignac and H. P. Cheng, *J. Chem. Phys.*, 2003, **118**, 10956–10962.
- M. Schmidt, A. Masson and C. Brechignac, *Phys. Rev. Lett.*, 2003, **91**, 243401.
- Y.-N. Wu, M. Schmidt, J. Leygnier, H.-P. Cheng, A. Masson and C. Brechignac, *J. Chem. Phys.*, 2012, **136**, 024314.



- 38 M. Schmidt, A. Masson, H.-P. Cheng and C. Brechignac, *ChemPhysChem*, 2015, **16**, 855–865.
- 39 M. Schmidt and C. Brechignac, *C. R. Phys.*, 2016, **17**, 481–484.
- 40 M. Arakawa, N. Hayashi, K. Minamikawa, T. Nishizato and A. Terasaki, *J. Phys. Chem. A*, 2022, **126**, 6920–6926.
- 41 J. van der Tol, D. Jia, Y. Li, V. Chernyy, J. M. Bakker, N. Minh Tho, P. Lievens and E. Janssens, *Phys. Chem. Chem. Phys.*, 2017, **19**, 19360–19368.
- 42 T. Wang, J. Ma, B. Yin and X. Xing, *J. Phys. Chem. A*, 2018, **122**, 3346–3352.
- 43 M. J. Frisch, G. W. Trucks, H. B. Schlegel, G. E. Scuseria and M. A. Robb, *et al.*, *Gaussian 09 Rev. C.01*, Wallingford, CT, 2010.
- 44 B. P. Pritchard, D. Altarawy, B. Didier, T. D. Gibson and T. L. Windus, *J. Chem. Inf. Model.*, 2019, **59**, 4814–4820.
- 45 D. Andrae, U. Haussermann, M. Dolg, H. Stoll and H. Preuss, *Theor. Chim. Acta*, 1990, **77**, 123–141.
- 46 F. Weigend and R. Ahlrichs, *Phys. Chem. Chem. Phys.*, 2005, **7**, 3297–3305.
- 47 H. L. Zhang and D. X. Tian, *Comput. Mater. Sci.*, 2008, **42**, 462–469.
- 48 Y. Y. Jin, Y. H. Tian, X. Y. Kuang, C. Z. Zhang, C. Lu, J. J. Wang, J. Lv, L. P. Ding and M. Ju, *J. Phys. Chem. A*, 2015, **119**, 6738–6745.
- 49 M. L. McKee and A. Samokhvalov, *J. Phys. Chem. A*, 2017, **121**, 5018–5028.
- 50 S.-Y. Yan, W. Zhang, Z.-X. Zhao, W.-C. Lu and H.-X. Zhang, *Theor. Chem. Acc.*, 2012, **131**, 1200.
- 51 L. Huang, W. Liu, J. Hu and X. Xing, *J. Phys. Chem. A*, 2021, **125**, 9995–10005.
- 52 B. E. Salisbury, W. T. Wallace and R. L. Whetten, *Chem. Phys.*, 2000, **262**, 131–141.
- 53 T. M. Bernhardt, J. Hagen, S. M. Lang, D. M. Popolan, L. D. Socaciu-Siebert and L. Woste, *J. Phys. Chem. A*, 2009, **113**, 2724–2733.
- 54 Z. Luo, C. Berkdemir, J. C. Smith and A. W. Castleman, *Chem. Phys. Lett.*, 2013, **582**, 24–30.

